Journal of Materials Chemistry A

Improving electrochemical performance of Li_2S cathode based on point defect control with cation/anion dual doping

Journal:	*Journal of Materials Chemistry A*
Manuscript ID	TA-ART-09-2023-005426.R1
Article Type:	Paper
Date Submitted by the Author:	25-Oct-2023
Complete List of Authors:	Wenli, Pan; Kyoto University, Graduate School of Human and Environment Studies Yamamoto, Kentaro; Kyoto University, Graduate School of Human and Environment Studies; Nara Women's University, Faculty of Engineering Machida , Nobuya; Konan Daigaku Rikogakubu, Department of Chemistry Matsunaga, Toshiyuki; Kyoto University, Graduate School of Human and Environmental Studies Kumar, Mukesh; Kyoto University, Graduate School of Human and Environment Studies Thakur, Neha; Kyoto University, Graduate School of Human and Environment Studies Watanabe, Toshiki; Kyoto University, Graduate School of Human and Environmental Studies Sakuda, Atsushi; Osaka Metropolitan University, Department of Applied Chemistry, Graduate School of Engineering Hayashi, Akitoshi; Osaka Metropolitan University, Department of Applied Chemistry, Graduate School of Engineering Tatsumisago, Masahiro; Osaka Metropolitan University, Department of Applied Chemistry, Graduate School of Engineering Uchimoto, Yoshiharu; Kyoto University, Graduate School of Human and Environmental Studies

ARTICLE

Improving electrochemical performance of Li_2S cathode based on point defect control with cation/anion dual doping

Received 00th January 20xx,
Accepted 00th January 20xx

DOI: 10.1039/x0xx00000x

Wenli Pan, [a] Kentaro Yamamoto,*[a,b] Nobuya Machida, [c] Toshiyuki Matsunaga, [a] Mukesh Kumar, [a] Neha Thakur, [a] Toshiki Watanabe, [a] Atsushi Sakuda, [d] Akitoshi Hayashi, [d] Masahiro Tatsumisago [d] and Yoshiharu Uchimoto [a]

Li_2S is a promising cathode candidate for all-solid-state batteries (ASSBs) because of its high theoretical capacity and availability of coupling with Li-free anode or anode less electrode. However, ionically insulating Li_2S leads to excess conductive additives, low sulfur utilization and sluggish kinetics, which hinders for ASSBs to implement the high energy density potential. Improving the intrinsic conductivity of Li_2S is the key to solve this issue. In this study, PI_3-doped Li_2S cathodes were synthesized and the relationship between lithium vacancies and ionic conductivities was examined quantitatively by time-of-flight (TOF) neutron diffraction. By cation-anion-dual doping, ionic conductivities of Li_2S-PI_3 materials were improved to 10^{-4} S cm^{-1}, which is capable for cathode without solid electrolytes added. Simply mixed with carbon, the Li_2S-PI_3-C cathode shows a high overall cathode capacity of 541 mAh g^{-1} with high S utilization of 82% at 0.05 C and capacity of 207 mAh g^{-1} at 1 C at room temperature, realizing high energy density with good rate performance.

Introduction

All-solid-state batteries (ASSBs) with sulfide-based solid electrolytes (SEs) are expected to be the next generation of storage batteries, because they possess potential with high energy density due to the bipolar structure, good power density due to the highly ion-conductive SE, and reliable safety due to the absence of organic solvents.[1-3] Among the cathode materials for ASSBs with sulfide electrolytes, Li_2S is a promising candidate due to its high theoretical capacity of 1167 mAh g^{-1} and the availability of Li-free anode such as Si and anode-less electrodes.[4, 5] However, because of extremely low ionic conductivity (10^{-9} S cm^{-1})[6, 7] and much insulation during charging with S_8 formation, it is necessary to mix Li_2S with a large amount of sulfide SEs as composite cathodes[8, 9]. These excessive SEs in the cathodes without contributing to capacity reduce the energy density of the whole cathode composites, which impedes the practical application of Li_2S-based cathodes for ASSBs with sulfide electrolytes.

In order to solve the issue, two types of methods have been widely studied: (1) to develop sulfide SEs with high ionic conductivity,[10, 11] and (2) to improve the apparent ionic conductivity of the cathode composites by increasing dispersion of sulfide SEs in cathode composites.[1, 12] As for the former one, several SE with high ionic conductivity have been developed, such as Li_6PS_5Cl,[13] $Li_7P_3S_{11}$,[14] $Li_{10}GeP_2S_{12}$,[15] $Li_{9.54}Si_{1.74}P_{1.44}S_{11.7}Cl_{0.3}$[16] and $Li_{9.54}[Si_{0.6}Ge_{0.4}]_{1.74}P_{1.44}S_{11.1}Br_{0.3}O_{0.6}$.[17] As for the later, different techniques have been used to fabricate composite electrodes with a liquid phase to control the dispersion state of the sulfide solid electrolytes in the cathode composites.[18-25] Although these approaches are effective in reducing the amount of sulfide SEs in cathode composites, the decomposition of SEs and the degradation at the cathode/SEs interface within the composite cathode during charging and discharging results in a continuous increase of impedance and poor cycling stability.[26, 27]

As a different approach from the methods mentioned above, several studies have been devoted to improve the ionic conductivity of Li_2S itself by controlling point defects in the structure.[28-31] It has been reported the insulting nature of Li_2S has associated with its stable antifluorite structure, which is consists of strong bond energy.[31] Therefore, point defect controlling by doping is probably capable of improving the ionic conductivity of Li_2S. Among different possible doping materials, lithium halide is proven to be effective in improving the ionic conductivity because of the introduction of lithium vacancies in Li_2S structure due to electrical neutrality. [28-31] In lithium halide doped Li_2S, it has been reported that LiI doped Li_2S (80Li_2S-20LiI) showed the ionic conductivity of 2×10^{-6} S cm^{-1} at 25 °C.[32-34] Recently, it has been reported that AlI_3 doped Li_2S (95Li_2S-5 AlI_3)

[a] Graduate School of Human and Environmental Studies, Kyoto University, Yoshida Nihonmatsu-cho, Sakyo, Kyoto 606-8501, Japan.
[b] Faculty of Engineering, Nara Women's University, Kitauoya-nishimachi, Nara, 630-8263, Japan
[c] Department of Chemistry of Functional Molecules, Konan University, Hyogo 658-8501, Japan.
[d] Department of Applied Chemistry, Graduate School of Engineering, Osaka Metropolitan University, Sakai, Osaka 599-8531, Japan
† Footnotes relating to the title and/or authors should appear here.
Electronic Supplementary Information (ESI) available: [details of any supplementary information available should be included here]. See DOI: 10.1039/x0xx00000x

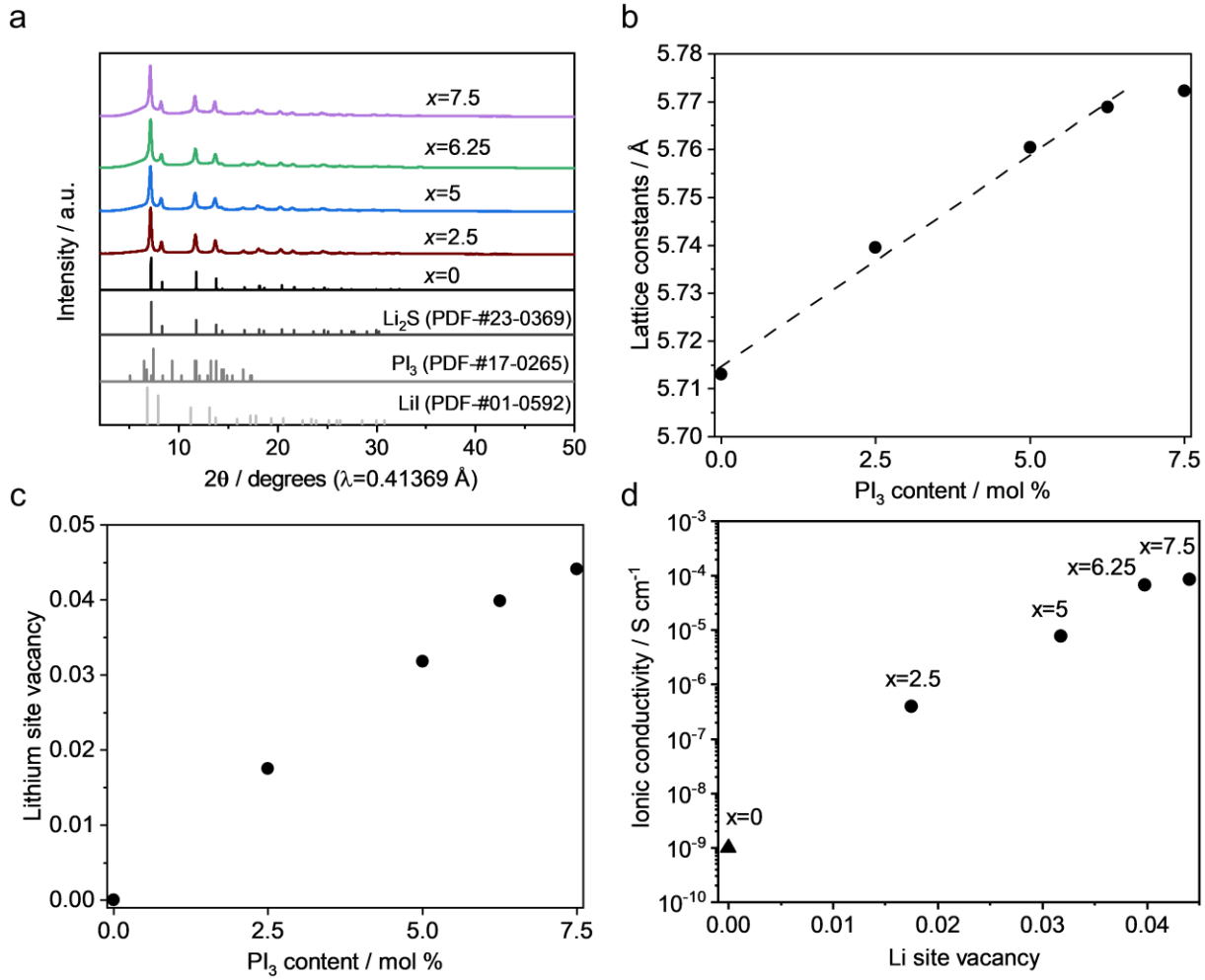

Fig. 1 Phase characterization of Li_2S-PI_3. (a) Synchrotron XRD patterns of (100-*x*) Li_2S-*x*PI_3 (*x* = 0, 2.5, 5, 6.25 and 7.5), with PI_3 and LiI for comparison. (b) The lattice constants of (100-*x*) Li_2S-*x*PI_3 (*x* = 0, 2.5, 5, 6.25 and 7.5) by Rietveld refinement of TOF neutron diffraction. (c) The relationship between PI_3 content of (100-*x*) Li_2S-*x*PI_3 (*x* = 0, 2.5, 5, 6.25 and 7.5) and Li vacancy. (d) The relationship between Li vacancy and ionic conductivities of (100-*x*) Li_2S-*x*PI_3 (*x*= 0, 2.5, 5, 6.25, 7.5). The ionic conductivity of Li_2S marked as triangle is cited as reported previously.[38]

showed a relatively higher ionic conductivity of 4.5×10^{-6} S cm^{-1} at room temperature because both Al^{3+} and I^- are dissolved into the Li_2S structure.[35] These results indicate that introducing lithium vacancies in the Li_2S structure by dual doping cation as well as anion with metal iodide is useful to improve the ionic conductivity of Li_2S. However, the relationship between the amount of the cation vacancy and ionic conductivity in metal-iodide-doped Li_2S has not been clearly understood because quantitative evaluation of cation vacancies has not been performed. Considering that S^{2-} is a soft Lewis base, it would be preferable to use a cation that is a soft Lewis acid to increase the amount of solid solution for the doped metal cation.

In this study, to address the above-mentioned issues, we prepared PI_3-doped Li_2S cathode materials and examined the relationship between the amount of the cation vacancy and ionic conductivity by using time-of-flight (TOF) neutron diffraction, which is sensitive to detect light element. It is found that the optimized Li_2S-PI_3 (93.5Li_2S-6.25PI_3) shows high ionic conductivity of 10^{-4} S cm^{-1}. Simply mixed with carbon, its composite shows a high overall cathode capacity of 541 mAh g^{-1} at 0.05 C and 207 mAh g^{-1} at 1 C under 25°C.

Experimental

Synthesis

The (100-*x*)Li_2S-*x*PI_3 samples (*x*=0, 2.5, 3, 4, 5, 6.25 and 7.5) in this study were prepared using ball milling. Stoichiometric amounts of Li_2S (99% purity, Aldrich) and PI_3 (99% purity, Aldrich) were hand-ground in a mortar for 0.5 h, followed by mechanical mixing with ZrO_2 balls at 530 rpm for 40 h. The Li_2S-PI_3-C cathode composites were prepared Li_2S-PI_3 samples and Cnovel MJ(4)030 (Toyo Tanso) with a 90:10 weight ratio by ball milling at 500 rpm for 10 h. The Li_3PS_4 glass powder used to fabricate the solid electrolyte layer with the ionic conductivity

of 5×10^{-4} S cm^{-1} was prepared via ball milling using a previously reported procedure.[36] Li_2S (99% purity, Aldrich) and P_2S_5 (99% purity, Aldrich) powders with a 3:1 molar ratio were mechanically mixed using ZrO_2 balls at 600 rpm for 16 h. All experiments were performed in a dry Ar-filled glovebox.

Characterization

The synchrotron X-ray diffraction (XRD) for the as-prepared (100-*x*)Li_2S-*x*PI_3 samples (*x* = 0, 2.5, 5, 6.25 and 7.5) was measured at the BL02B2 beamline at SPring-8, Japan. Time-of-flight (TOF) neutron diffraction was conducted on (100-*x*)Li_2S-*x*PI_3 samples (*x*=0, 2.5, 5, 6.25, 7.5) at BL20 (iMATERIA) beamline in J-PARK, Japan. The Rietveld refinement was performed with Jana.[37] And these Li_2S-PI_3 samples were also measured by photoelectron spectroscope (XPS, VersaProbe Ⅲ). Scanning electron microscope (SEM, Hitachi SU-8220) and energy dispersive X-ray spectroscopy (EDS, Horiba X-max^N) mapping were used for (100-*x*)Li_2S-*x*PI_3 samples (*x* = 0, 2.5, 5, 6.25, 7.5) and the cross section of the 93.75Li_2S-6.25PI_3-C/Li_3PS_4 pellet. The X-ray absorption spectroscopy (XAS) of S *K*-edge for the cathode materials after galvanostatic measurements was measured without air exposure at the BL6N1 beamline of the Aichi Synchrotron Radiation Center, Japan.

Electrochemistry measurements

The electrochemical performance of the Li_2S-PI_3-C cathode materials was analyzed using a two-electrode cell. The Li_2S-PI_3-C composites were used as cathode materials without adding solid electrolyte to them, and the prepared Li_3PS_4 was used as the solid electrolyte layer of the cell. The Li_2S-PI_3-C cathode materials (4 mg) and the Li_3PS_4 (80 mg) for solid electrolyte layer were placed in a polycarbonate tube with a diameter of 10 mm and were pressed under a pressure of 360 MPa. The cross-section SEM and EDS mapping for Li_2S-PI_3-C/Li_3PS_4 pellet shown in Fig. S1, † that the Li_3PS_4 layer, with a thickness of about 550 μm, is uniformly covered by Li_2S-PI_3-C, which has the thickness of 28 μm" and "All the calculations for specific capacities are based on the mass of cathode composites. 1 C is the weight proportion of Li_2S in Li_2S-PI_3-C cathode times theoretical capacity of Li_2S (1167 mAh g^{-1}). A Li–In alloy layer was placed on the solid electrolyte at the opposite side to the cathode layer and served as the anode[38]. Two stainless-steel rods, which were added to the cathode and anode sides by applying a pressure of 120 MPa, were used as current collectors. The cell assembly was performed in a dry Ar-filled glovebox. Electrochemical tests for the cells were performed with discharge and charge cutoff voltages of 0 (0.62 V vs. Li) and 3.0 V (3.62 V vs. Li), respectively, at 25 °C. All the calculations for specific capacities are based on the mass of cathode composites. 1 C is the weight proportion of Li_2S in Li_2S-PI_3-C cathode times theoretical capacity of Li_2S (1167 mAh g^{-1}). Alternating current (AC) impedance was conducted to measure the ionic conductivities of the (100-*x*)Li_2S-*x*PI_3 by using Modulab XM ECS (Solartron Analytical). The materials were loaded into a polycarbonate tube with a diameter of 10 mm and pressed into pellets under a pressure of 360 MPa and set between two stainless-steel current collector plates. The AC amplitude was 10 mV, and the applied frequency ranged between 1 MHz and 0.1 Hz.

Results and discussion

The crystal structures of (100-*x*)Li_2S-*x*PI_3 (*x* = 0, 2.5, 5, 6.25, and 7.5) were examined by synchrotron XRD and TOF neutron diffraction. In the synchrotron XRD (Fig. 1a), all sharp peaks of (100-*x*)Li_2S-*x*PI_3 (*x* = 0, 2.5, 5, 6.25) were assigned to Li_2S (space group: $Fm\bar{3}m$) while a broad peak appeared around 7.1° in addition to the sharp peaks might attributed to PI_3 or LiI in the 92.5Li_2S-7.5PI_3 (*x* = 7.5). The lattice constants and site occupancy of each element in the (100-*x*)Li_2S-*x*PI_3 (*x* = 0, 2.5, 5, 6.25 and 7.5) were calculated by Rietveld analysis for the neutron diffraction patterns because the neutron beam is more sensitive to light element such as lithium than X-ray (Fig. 1b-c, Fig. S2†, Table S1†). In order to obtain more accurate results, refinement conducted on the series of Li_2S-PI_3 samples was based on all of QA, BS and LA bank data. As shown in Fig. 1b and 1c, both lattice constant and lithium site vacancy of (100-*x*)Li_2S-*x*PI_3 increased linearly with the increment of PI_3 content up to *x* = 6.25, and increased slightly from *x* = 6.25 to *x* = 7.5. The linear lattice expansion with PI_3 content is because PI_3 was doped into the Li_2S structure with the substitution of larger I^- (ionic radii: 2.2 Å) than S^{2-} (ionic radii: 1.84 Å).[39] The P^{3+} and I^- occupied the lithium site and sulfur site in the Li_2S structure, respectively, leading to the linearly increased lithium site vacancy for compensation to keep the electrical neutrality (Fig. 1c and Table S1†). The minor change of lattice constant and lithium site vacancy from *x* = 6.25 to *x* = 7.5 indicates that a solid solution limit exists between *x* = 6.25 and *x* = 7.5, which is in agreement with the observation of the broad peak in the sample with *x* = 7.5 in XRD. Besides, XPS S 2p, P 2p and I 3d measurements have been conducted for (100-*x*)Li_2S-*x*PI_3 (*x* = 0, 2.5, 5, 6.25 and 7.5) samples to confirm the formation of solid solution further, which shown in Fig. S4†. In the P 2p and I 3d regions, no peak was observed in the sample with *x* = 0 but a peak was observed at 132.4 eV and 619.1 eV, respectively, with addition of PI_3 (*x* =2.5, 5, 6.25 and 7.5). The peak intensity in the P 2p and I 3d regions increased from *x* = 4 to *x* = 6.25 and slightly increase from *x* = 6.25 to *x* = 7.5. In the S 2p region, two peaks attributed to $S2p_{1/2}$ and $S2p_{3/2}$ were observed around 160.0 eV and 161.2 eV [40, 41] in the sample with *x* = 0. The binding energy of the two peaks shifted to higher energy with increase of *x* value. These results indicate the change of electronic structure of S in Li_2S with doping,[35] which supports the formation of solid solution further.

To examine the effect of the crystal structure of (100-*x*)Li_2S-*x*PI_3 on its ionic conductivity, AC impedance spectroscopy at 25°C was performed for (100-*x*)Li_2S-*x*PI_3 (*x* = 2.5, 3, 4, 5, 6.25 and 7) (Fig. S5 †). Fig. 1d shows a plot between the ionic conductivities and lithium site vacancy of the (100-*x*)Li_2S-*x*PI_3 (*x* = 0, 2.5, 5, 6.25 and 7.5). The ionic conductivity of (100-*x*)Li_2S-*x*PI_3 was largely increased from 10^{-9} S cm^{-1} with increase of lithium site vacancy to 6.8×10^{-5} S cm^{-1} (*x* = 6.25) and increased

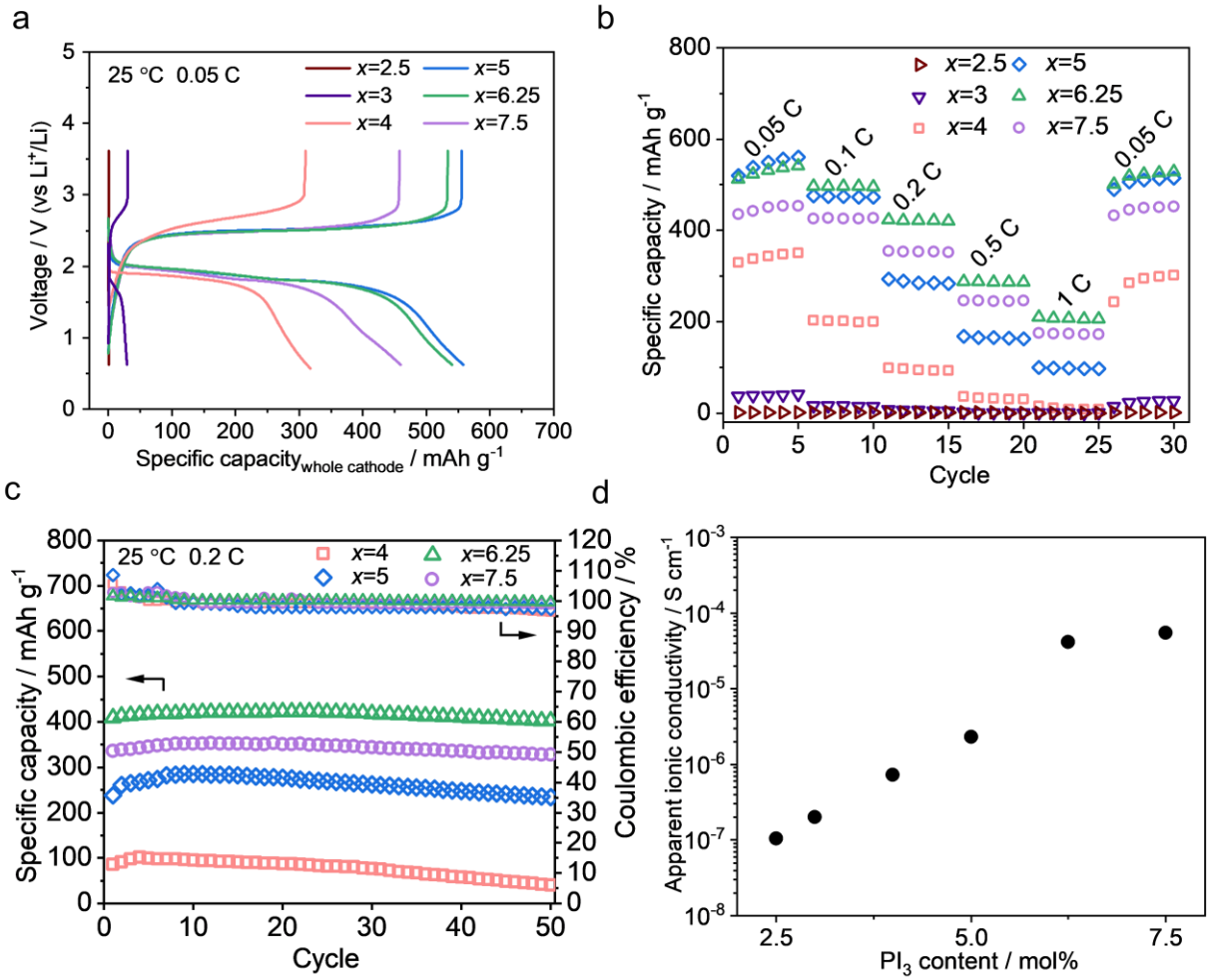

Fig. 2 The electrochemical performance of (100-*x*)Li_2S-*x*PI_3-C (*x* = 2.5, 3, 4, 5, 6.25, 7.5) cathode composites. Specific capacities were calculated based on the overall mass of cathode. (a) Galvanostatic charge-discharge curves at 0.05 C. (b) The specific capacities at different C-rates. (c) Cycling stability at 0.2 C. (d) The apparent ionic conductivity for first full charge. All the calculations for specific capacities are based on the mass of cathode composites. 1 C is the weight proportion of Li_2S in Li_2S-PI_3-C cathode times theoretical capacity of Li_2S (1167 mAh g^{-1}).

slightly to 8.5 × 10^{-5} S cm^{-1} (*x* = 7.5) (Fig. 1d). The particle sizes shown in Fig. S2† of (100-*x*)Li_2S-*x*PI_3 (*x* = 2.5, 5, 6.25 and 7.5) were similar with a few micrometers, indicating that they did not influence the ionic conductivity.The ionic conductivity of ~10^{-4} S cm^{-1} has the same order of magnitude as that of Li_3PS_4, which is a typical solid electrolyte for all-solid-state batteries.[42, 43] Therefore, it is possible to take advantage of high-conductivity Li_2S-PI_3 for cathode materials without SE.

To evaluate the electrochemical performance, the (100-*x*)Li_2S-*x*PI_3 (*x* = 2.5, 3, 4, 5, 6.25 and 7.5) samples were mixed with CNovel as electron additive to prepare cathode composites, in which the ratio of (100-*x*)Li_2S-*x*PI_3 : CNovel = 9:1 wt%. The galvanostatic charge-discharge curves at 0.05 C under 25°C are shown in Fig. 2a. The (100-*x*)Li_2S-*x*PI_3-C cathode *x*=2.5 did not deliver any capacity probably because of the insufficient ionic conductivity shown in Fig. 1d. The (100-*x*)Li_2S-*x*PI_3-C cathode with higher PI_3 content than *x* = 2.5 exhibited reversible charge/discharge curves with a single plateau for each process. The dQ/dV plot obtained from Fig. 2a (Fig. S6†) shows one peak during the charge process around 2.6 V in each sample. The voltage corresponds to the typical transformation of Li_2S to S_8 via polysulfides,[44] meaning that the PI_3 doping does not provide an additional reaction in the cathode composites. The discharge capacities for cathodes with *x* = 3, 4, 5, 6.25 and 7.5 were 30, 319, 560, 541 and 459 mAh g^{-1}. The rate capability of the (100-*x*)Li_2S-*x*PI_3-C cathodes was measured at 0.05, 0.1, 0.2, 0.5 and 1 C (Fig. 2b). Although the (100-*x*)Li_2S-*x*PI_3-C cathode with *x* = 5 showed the highest capacity at the low rate of 0.05 C, the capacity retention at higher rates increased with the amount of PI_3 contents. It is because the Li_2S content in the electrode decreases with increasing PI_3 content despite the improved ionic conductivity (Fig. 1d). Among them, the (100-x)Li_2S-xPI_3-C cathode with *x* = 6.25 achieved both high capacity and good rate performance The charge-discharge capacity remains stable at various current densities. The (100-x)Li_2S-xPI_3-C with *x* = 6.25 provided a discharge capacity of 541 mAh g^{-1} at 0.05 C and 207 mAh g^{-1} 1 C (1 C = 657 mAh g^{-1}), respectively. As evident from Fig. 2b, the capacity values are significantly higher than those of

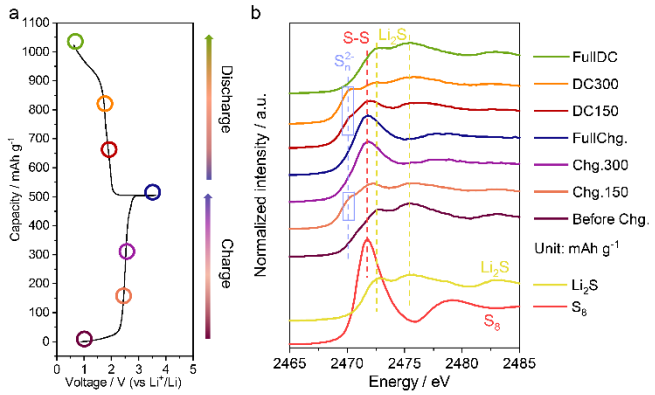

Fig. 3 Reaction mechanism of 93.75Li_2S-6.25PI_3-C. (a) Charge-discharge curves at different state during second cycle (b) Corresponding S K-edge XANES spectra during second cycle, with Li_2S and S_8 as standard materials.

other cathode materials. After the C-rate is dropped back to 0.05 C, the capacity increased to 528 mAh g^{-1}, showing good reversibility after charge-discharge process at high C-rates. Meanwhile, the (100-*x*)Li_2S-*x*PI_3-C with *x* = 6.25 maintained satisfied cycling stability of 95% after 50 cycles, with an average Columbic efficiency of 99.8% from 31st cycle to 50th cycle, while 96Li_2S-4PI_3-C maintained only 39 % of its initial capacity after 50 cycles, which supports the improved performance with PI_3 doping and the effectiveness of creating point defect in Li_2S. To better understand the improved rate performance on the battery level, the EIS measurements were conducted for those batteries with (100-*x*)Li_2S-*x*PI_3-C cathode (*x* = 4, 5, 6.25 and 7.5) at pristine state. The proper equivalent circuit model has been fitted for EIS data (shown in Fig. S7†, S8† and Table S2†). A semicircle was observed in each battery and the resistance of semicircle is attributed to charge transfer resistance (R_{ct}) It is because capacitances of those samples were 10^{-6} to 10^{-5} F,[45,46] which were assigned to be interface between the Li_2S-PI_3-C cathodes and Li_3PS_4 SE layer. The values of R_{ct} decreased with PI_3 content, demonstrating faster ion transport through the interface, which benefits rate performance. Moreover, the apparent ionic conductivities for (100-*x*)Li_2S-*x*PI_3 (*x* = 2.5, 3, 4, 5, 6.25 and 7.5) at first full-charge state were measured based on Cottrell and Nernst—Einstein equations (Fig. 2d, Fig.S9†). The apparent ionic conductivity was significantly increased with increase of PI_3 content up to *x* = 6.25 and increased slightly from *x* = 6.25 to *x* = 7.5. The apparent ionic conductivities of (100-*x*)Li_2S-*x*PI_3 (*x* = 6.25 and 7.5) were relatively high (4.1×10^{-5} S cm^{-1} for the cathode with *x* = 6.25). This means that these cathodes kept high effective ionic conductivity at charging state, leading to the good rate performance. Based on the discussion above, the capacities on the cathode level, rate performance, cycling stability, and effective ionic conductivities at full-charge state are all improved with introducing point defects in Li_2S structure, which proves our strategy is feasible.

To examine charge compensation mechanism of the (100-*x*)Li_2S-*x*PI_3 with *x* = 6.25, which is optimized sample, XAS for S *K*-edge was performed (Fig. 3). Before charge process, two characteristic peaks attributed to Li_2S[47] were observed at 2472.6 and 2475.3 eV. When charging to 150 mAh g^{-1}, the intensity of the peaks assigned to Li_2S at 2472.6 and 2475.3 eV was decreased while two peaks appeared at 2470.2 and 2471.8 eV. These two peaks at 2470.2 and 2471.8 eV were assigned to the S 1s to π^* state transition associated with polysulfides[48] and the S 1s to S-S π^* state transition of element sulfur[43], respectively. For the further charge, the peaks assigned to Li_2S and polysulfides showed decrease in intensity while the intensity of the peak assigned to S_8 at 2471.8 eV was increased. These results indicate the charge compensation during charging results from the transformation from Li_2S to S_8 via polysulfide in the cathode. For the discharge process to 300 mAh g^{-1}, the intensity of the peak assigned to S_8 at 2471.8 eV was decreased while those of the peaks assigned to polysulfides and Li_2S were increased, indicating S_8 is under the lithiation process. For the further discharge, the intensity of the peaks assigned to polysulfides and S_8 was decreased and the peaks assigned to Li_2S remained increased. The spectrum of the cathode at the full charge state was in good agreement with that of the cathode at the before charge state. These results show that the transformation between Li_2S and S_8 with polysulfide occurred reversibly, corresponding to the good reversibility in the charge/discharge cycling.

Finally, the energy density and power density of the 93.75Li_2S-6.25PI_3-C cathode based on overall cathode weight were compared with other conventional cathodes for all-solid-state Li-S batteries (Fig. 4).[28, 35, 49-54] Among them, the 93.75Li_2S-6.25PI_3-C cathode shows highest energy density and power density. These results are due to the fact that controlling defects in Li_2S through cation/anion dual doping dramatically increased the ionic conductivity of Li_2S itself, and thereby reduced the amount of sulfide solid electrolyte in the cathode composite.

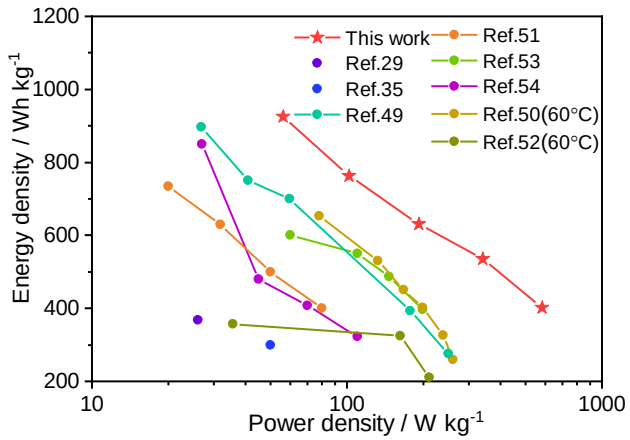

Fig. 4 Comparison among different cathode composites for all-solid-state Li-S batteries for their energy densities and power densities of different cathode composites at cathode level.

Conclusions

In this study, (100-*x*)Li_2S-*x*PI_3 cathodes were synthesized by ball-milling method. TOF neutron diffraction and ionic conductivity

measurement proves the ionic conductivity of the (100-*x*)Li_2S-*x*PI_3 is improved by formation of lithium vacancies with the increase of PI_3 content. The PI_3 content-optimized 93.75Li_2S-6.25PI_3 shows good ionic conductivity around 10^{-4} S cm^{-1}, which is capable for cathode without SEs. Under 25 ℃, the the 93.75Li_2S-6.25PI_3-C cathode composite shows a high overall cathode capacity of 541 mAh g^{-1} with high S utilization of 82% at 0.05 C. It delivers 207 mAh g^{-1} at 1 C and shows high reversibility after high current density. The XAS for S K-edge confirms that the charge compensation of the cathode is performed by the transformation between Li_2S and S_8 with polysulfide and the transformation is reversible. The lithium site vacancy in Li_2S structure can be controlled precisely by PI_3 doping, improving the ionic conductivity drastically enough to use the Li_2S-PI_3 as cathode without SE. The developed high-performance Li_2S-PI_3-C cathode shows the successful strategy of cation-anion dual doping, which paves the way for practical application of ASSBs at room temperature.

Author Contributions

W. Pan collected data, performed analysis and wrote the manuscript. K. Yamamoto validated data, supervised the project and revised the draft. N. Machida conceived the strategy. T. Matsunaga conducted crystal structure analysis. M. Kumar and N. Thakur revised the manuscript. T. Watanabe performed analysis. A. Sakuda, A. Hayashi and M. Tatsumisago conducted and supported measurements. Y. Uchimoto validated data, supervised the project, provided resources and revised the manuscript.

Conflicts of interest

There are no conflicts to declare

Acknowledgements

This research was supported by JST, ALCA-SPRING Project (Grant Number: JPMJAL1301). Synchrotron radiation experiments were performed at beam line BL02B2 at SPring-8 with the approval of the JASRI (Proposal numbers 2020A0664 and 2022A1781) and BL6N1 at Aichi SR (Proposal numbers 202206124). The neutron diffraction experiments were conducted as an S-type project of KEK (Proposal No. 2019S10). Acknowledgement is also issued to China Scholarship Council (No. 202208050074) for its financial support to W. Pan.

References

1 J. Wu, S. Liu, F. Han, X. Yao and C. Wang, *Adv. Mater.*, 2021, **33**, 2000751.
2 C. Wang, J. Liang, Y. Zhao, M. Zheng, X. Li and X. Sun, *Energy Environ. Sci.*, 2021, **14**, 2577-2619.
3 C. Wang, J. T. Kim, C. Wang and X. Sun, *Adv. Mater.*, 2023, **35**, 2209074.
4 L. Wang, Y. Wang and Y. Xia, *Energy Environ. Sci.*, 2015, **8**, 1551-1558.
5 J. Xiang, Y. Zhao, L. Wang and C. Zha, *J. Mater. Chem. A*, 2022, **10**, 10326-10341.
6 Y. Yang, G. Zheng and Y. Cui, *Chem. Soc. Rev.*, 2013, **42**, 3018-3032.
7 F. Altorfer, W. Bührer, I. Anderson, O. Schärpf, H. Bill, P. Carron and H. Smith, *Phys. B: Condens. Matter*, 1992, **180**, 795-797.
8 S. H. Chung, C. H. Chang and A. Manthiram, *Adv. Funct. Mater.*, 2018, **28**, 1801188.
9 R. Fang, S. Zhao, Z. Sun, D. W. Wang, H. M. Cheng and F. Li, *Adv. Mater.*, 2017, **29**, 1606823.
10 H. Yang and N. Wu, *Energy Sci. Eng.*, 2022, **10**, 1643-1671.
11 Y. Wang, Y. Wu, Z. Wang, L. Chen, H. Li and F. Wu, *J. Mater. Chem. A*, 2022, **10**, 4517-4532.
12 M. Ali, C.-H. Doh, Y.-J. Lee, B.-G. Kim, J.-W. Park, J. Park, G. Park, W.-J. Lee, S.-M. Lee and Y.-C. Ha, *Energy Technol.*, 2021, **9**, 2001096.
13 C. Hänsel and D. Kundu, *Adv. Mater. Interfaces*, 2021, **8**, 2100206.
14 D. Chang, K. Oh, S. J. Kim and K. Kang, *Chem. Mater*, 2018, **30**, 8764-8770.
15 N. Kamaya, K. Homma, Y. Yamakawa, M. Hirayama, R. Kanno, M. Yonemura, T. Kamiyama, Y. Kato, S. Hama and K. Kawamoto, *Nat. Mater*, 2011, **10**, 682-686.
16 Y. Kato, S. Hori, T. Saito, K. Suzuki, M. Hirayama, A. Mitsui, M. Yonemura, H. Iba and R. Kanno, *Nat. Energy*, 2016, **1**, 1-7.
17 Y. Li, S. Song, H. Kim, K. Nomoto, H. Kim, X. Sun, S. Hori, K. Suzuki, N. Matsui and M. Hirayama, *Science*, 2023, **381**, 50-53.
18 S. Teragawa, K. Aso, K. Tadanaga, A. Hayashi and M. Tatsumisago, *J. Mater. Chem. A*, 2014, **2**, 5095-5099.
19 S. Yubuchi, S. Teragawa, K. Aso, K. Tadanaga, A. Hayashi and M. Tatsumisago, *J. Power Sources*, 2015, **293**, 941-945.
20 N. H. H. Phuc, K. Morikawa, T. Mitsuhiro, H. Muto and A. Matsuda, *Ionics*, 2017, **23**, 2061-2067.
21 N. C. Rosero-Navarro, T. Kinoshita, A. Miura, M. Higuchi and K. Tadanaga, *Ionics*, 2017, **23**, 1619-1624.
22 N. C. Rosero-Navarro, A. Miura and K. Tadanaga, *J. Power Sources*, 2018, **396**, 33-40.
23 Y.-J. Yen and S.-H. Chung, *J. Mater. Chem. A*, 2023, **11**, 4519-4526.
24 A. Le Mong and D. Kim, *J. Mater. Chem. A*, 2023, **11**, 6503-6521.
25 R. Zhao, J. Yang, X. Han, Y. Wang, Q. Ni, Z. Hu, C. Wu and Y. Bai, *Adv. Energy Mater.*, 2023, **13**, 2203542
26 T. Brahmbhatt, G. Yang, E. C. Self and J. Nanda, *Front. Energy Res.*, 2020, **8**, 570754.
27 Y. Morino, H. Tsukasaki and S. Mori, *ACS Appl. Mater. Interfaces*, 2023, **15**, 23051-23057.
28 W. Qu, Z. Lu, C. Geng, L. Wang, Y. Guo, Y. Zhang, W. Wang, W. Lv and Q. H. Yang, *Adv. Energy Mater.*, 2022, **12**, 2202232.
29 T. Hakari, A. Hayashi and M. Tatsumisago, *Adv. Sustain. Syst.*, 2017, **1**, 1700017.
30 T. Hakari, A. Hayashi and M. Tatsumisago, *Chem. Lett.*, 2015, **44**, 1664-1666.
31 C. Zha, S. Wang, C. Liu, Y. Zhao, B. He, C. Lyu, J. Li, S. Ji, S. Chen, K. S. Hui and K. N. Hui, *Energy Storage Mater.*, 2022, **47**, 79-86.
32 Y. Fujita, T. Hakari, A. Sakuda, M. Deguchi, Y. Kawasaki, H. Tsukasaki, S. Mori, M. Tatsumisago and A. Hayashi, *ACS Appl. Energy Mater.*, 2022, **5**, 9429-9436.
33 J. T. Kim, X. Hao, C. Wang and X. Sun, *Matter*, 2023.
34 F. Wu, J. T. Lee, N. Nitta, H. Kim, O. Borodin and G. Yushin, *Adv. Mater.*, 2015, **27**, 101-108.
35 H. Gamo, T. Maeda, K. Hikima, M. Deguchi, Y. Fujita, Y. Kawasaki, A. Sakuda, H. Muto, N. H. H. Phuc and A. Hayashi, *Mater. Adv.*, 2022, **3**, 2488-2494.

36 K. Yamamoto, S. Yang, M. Takahashi, K. Ohara, T. Uchiyama, T. Watanabe, A. Sakuda, A. Hayashi, M. Tatsumisago and H. Muto, *ACS Appl. Energy Mater.*, 2021, **4**, 2275-2281.
37 V. Petříček, M. Dušek and L. Palatinus, *Z. Krist. Cryst. Mater.*, 2014, **229**, 345-352.
38 A. Santhosha, L. Medenbach, J. R. Buchheim and P. Adelhelm, *Batter. Supercaps*, 2019, **2**, 524-529.
39 R. D. Shannon, *Acta Crystallogr., Sect. A: Cryst. Phys., Diffr., Theor. Gen. Crystallogr.*, 1976, **32**, 751-767.
40 Y. Fujita, T. Hakari, A. Sakuda, M. Deguchi, Y. Kawasaki, H. Tsukasaki, S. Mori, M. Tatsumisago and A. Hayashi, *ACS Appl. Energy Mater.*, 2022, **5**, 9429-9436.
41 Q. Fan, J. Jiang, S. Zhang, T. Zhou, W. K. Pang, Q. Gu, H. Liu, Z. Guo and J. Wang, *Adv. Energy Mater.*, 2021, **11**, 2100957.
42 Z. Liu, W. Fu, E. A. Payzant, X. Yu, Z. Wu, N. J. Dudney, J. Kiggans, K. Hong, A. J. Rondinone and C. Liang, *J. Am. Chem. Soc.*, 2013, **135**, 975-978.
43 H. Stöffler, T. Zinkevich, M. Yavuz, A.-L. Hansen, M. Knapp, J. Bednarčík, S. Randau, F. H. Richter, J. Janek, H. Ehrenberg and S. Indris, *J. Phys. Chem. C*, 2019, **123**, 10280-10290.
44 L. Zhang, D. Sun, J. Feng, E. J. Cairns and J. Guo, *Nano Lett.*, 2017, **17**, 5084-5091.
45 J. T. Irvine, D. C. Sinclair and A. R. West, *Adv. Mater.*, 1990, **2**, 132-138.
46 W. Zhang, D. A. Weber, H. Weigand, T. Arlt, I. Manke, D. Schröder, R. Koerver, T. Leichtweiss, P. Hartmann and W. G. Zeier, *ACS Appl. Mater. Interfaces*, 2017, **9**, 17835-17845.
47 E. Zhao, J. Wang, F. Li, Z. Jiang, X. Q. Yang, F. Wang, H. Li and X. Yu, *Chem. Commun.*, 2019, **55**, 4993-4996.
48 M. Cuisinier, P.-E. Cabelguen, S. Evers, G. He, M. Kolbeck, A. Garsuch, T. Bolin, M. Balasubramanian and L. F. Nazar, *J. Phys. Chem. Lett.*, 2013, **4**, 3227-3232.
49 J. P. Mwizerwa, Q. Zhang, F. Han, H. Wan, L. Cai, C. Wang and X. Yao, *ACS Appl. Mater. Interfaces*, 2020, **12**, 18519-18525.
50 H. Yan, H. Wang, D. Wang, X. Li, Z. Gong and Y. Yang, *Nano lett.*, 2019, **19**, 3280-3287.
51 Y. Zhang, T. Liu, Q. Zhang, X. Zhang, S. Wang, X. Wang, L. Li, L.-Z. Fan, C.-W. Nan and Y. Shen, *J. Mater. Chem. A*, 2018, **6**, 23345-23356.
52 X. Yao, N. Huang, F. Han, Q. Zhang, H. Wan, J. P. Mwizerwa, C. Wang and X. Xu, *Adv. Energy Mater.*, 2017, **7**, 1602923.
53 Q. Zhang, N. Huang, Z. Huang, L. Cai, J. Wu and X. Yao, *J. Energy Chem.*, 2020, **40**, 151-155.
54 L.-P. Hou, H. Yuan, C.-Z. Zhao, L. Xu, G.-L. Zhu, H.-X. Nan, X.-B. Cheng, Q.-B. Liu, C.-X. He and J.-Q. Huang, *Energy Storage Mater.*, 2020, **25**, 436-442.